Spatial downscaling of radar-derived rainfall field by two-dimensional wavelet transform

Vahid Nourani, Armin Farshbaf and S. Adarsh

ABSTRACT

Downscaling of rainfall fields, either as images or products of global circulation models, have been the motive of many hydrologists and hydro-meteorologists. The main concern in downscaling is to transform high-resolution properties of the rainfall field to lower resolution without introducing erroneous information. In this paper, rainfall fields obtained from Next Generation Weather Surveillance Radar (NEXRAD) Level III were examined in the wavelet domain which revealed sparsity for wavelet coefficients. The proposed methodology in this work employs a concept named Standardized Rainfall Fluctuation (SRF) to overcome the sparsity of rainfall fields in wavelet domain which also exhibited scaling behaviors in a range of scales. SRFs utilizes such scaling behaviors where upscaled versions of the rainfall fields are downscaled to their actual size, using a two-dimensional discrete wavelet transform, to examine the reproduction of the rainfall fields. Furthermore, model modifications were employed to enhance the accuracy. These modifications include removing the negative values while conserving the mean and applying a non-overlapping kernel to restore high-gradient clusters of rainfall fields. The calculated correlation coefficient, statistical moments, determination coefficient and spatial pattern display a good agreement between the outputs of the downscaling method and the observed rainfall fields.

Key words | scaling behavior, spatial downscaling, wavelet transform, weather surveillance radar

Vahid Nourani (corresponding author)
Armin Farshbaf
Center of Excellence in Hydroinformatics,
Faculty of Civil Engineering,
University of Tabriz,
Tabriz,
Iran
E-mail: *vnourani@yahoo.com*

Vahid Nourani
Faculty of Civil and Environmental Engingeering,
Near East University,
via Mersin 10., Nicosia,
Turkey

S. Adarsh
Department of Civil Engineering,
TKM College of Engineering,
Kollam,
India

INTRODUCTION

Precipitation is a key component of the water cycle as a very important research topic in the atmospheric and hydrologic sciences. Precipitation is also one of the most difficult variables to estimate accurately in hydrological, hydro-meteorological and climatological models due to its complex and stochastic nature. Nowadays, researchers try to reduce the extent of uncertainty in their works using high-resolution rainfall data. High-resolution rainfall fields are also essential for understanding the response of small watersheds, especially hydrologic extremes, since these types of watersheds are sensitive to small variations of rainfall (e.g. Rebora *et al.* 2006). Unfortunately, these types of data are limited to specific locations and for a small period which implies that an alternative way to obtain the necessary high-resolution rainfall data is needed. The main approach for acquiring the necessary rainfall data is transforming the available rainfall data into the required resolution. In other words, there is a dire need for downscaling methods. One of the major challenges in rainfall downscaling is accounting for the average amount of rainfall while preserving extreme values of rainfall (Koutsoyiannis & Onof 2001).

doi: 10.2166/nh.2020.165

Rainfall downscaling is applicable at both temporal and spatial scales. Temporal rainfall downscaling methods aim at increasing the overall count of pulses of rainfall or, in other terms, reducing the duration of each pulse of rainfall (Ormsbee 1989; Farboudfam & Nourani 2018; Nourani & Farboudfam 2019). Unlike temporal rainfall downscaling, methods for spatial rainfall downscaling are slim and are mostly focused on using interpolations techniques (Kang & Ramrez 2010).

Rain measurement devices such as rain gauges and radars have various problems regarding available data. Rain gauges usually store data at a daily resolution which lacks the sufficient resolution for various hydrological applications (Singh 1997). Also, they are extremely sensitive to wind velocity above the gauge, water splashing out of the gauge, evaporation and, most importantly, their inability to represent spatial precipitation (WMO 2008). To date, different methods using networks of rain gauges have been developed to represent spatial variation of rainfall such as Thiessen polygon, arithmetic mean, Isohyetal, Spline and Kriging (Chow *et al.* 1988; AghaKouchak *et al.* 2010), but such methods tend to underestimate high-resolution variability (Singh & Chowdhury 1986). Moreover, one of the fields that require downscaling methods to address the problem of resolution discrepancy acquired by various precipitation measurement instruments (e.g. rain gauge, satellites, weather surveillance radars) is data-fusion (Ebtehaj & Foufoula-Georgiou 2011a, 2011b; Cammalleri *et al.* 2013).

The structure of precipitation both in time and space at different resolutions has undergone various investigations via different methods (e.g. López López 2018; Baghanam *et al.* 2019). One of these methods is based on point process techniques which resulted in rectangular pulse models of Neyman-Scott and Bartlett-Lewis developed by Rodriguez-Iturbe *et al.* (1987, 1988) and later improved by other researchers (Cowpertwait *et al.* 1996; Koutsoyiannis & Onof 2001). Another method called the random cascade process was widely used which repeatedly divides each point of rainfall field to smaller fields, whether in space or time domain. This method is based on scale-invariant behavior of rainfall in a wide range of scales which suggests that rainfall fields at various scales are related through a power law also known as scaling (Olsson 1995). This process can only be applied to some specific scales of the rainfall field. In general, scaling in rainfall can be identified as having a log-log linear relationship between statistical moments in various spectrums (Lovejoy & Schertzer 1990; Kumar & Foufoula-Georgiou 1993a, 1993b; Venugopal *et al.* 2006). This study aims at overcoming the limitations of existing methods by proposing an approach based on wavelet transform to examine the rainfall fields at various resolutions.

A detailed literature review demonstrated that although some works have been carried out to predict the variability of spatial rainfall, there are many uncertainties regarding high-resolution rainfall data. Hence, the main purpose of this paper is to demonstrate: (1) the scaling behavior of a wide range of rainfall events with different shapes and spatial patterns; and (2) introduce a downscaling framework using the wavelet transform. Evaluation of the proposed model is performed using various statistical criteria.

MATERIALS AND METHODS

In this section, a brief explanation of weather surveillance radars, obtained data-set, properties of wavelet transform, scaling behavior of rainfall fields in the wavelet domain, as well as the process of downscaling and its implementation, is presented.

In recent decades, weather surveillance radars such as Next Generation Radars (NEXRAD) have been used to measure precipitation (Berne & Krajewski 2013). The primary reason for choosing NEXRAD outputs instead of other forms of rainfall retrieval mediums is its high resolution which is a necessary aspect to understanding rainfall properties. These radars emit pulses of microwave energy into the atmosphere where these beams collide with objects such as raindrops, hail, and snowflakes. Afterward, some of the energy bounces back towards the radar to be collected. Base reflectivity is the main product of Doppler weather radars which displays the amount of power returned to the radar after being reflected from the atmosphere. Base reflectivity is measured in decibels (dBZ). In order to convert radar reflectivity into rainfall intensities, the experimental Z-R relations that are in the form of $Z = aR^b$ are used in which Z is the reflectivity factor expressed in $mm^6\,m^{-3}$ (1 dBZ = 10 log-Z), R is the rainfall intensity in units of

mm hr^{-1} and the parameters (a, b) are related to drop size distribution. A list of Z-R equations has been recommended by the Radar Operations Center for different forms of precipitation (Joss & Waldvogel 1990). It is worth noting that based on previous studies various Z-R equations had insignificant impacts on the final results of the downscaling process (Perica & Foufoula-Georgiou 1996a). Therefore, the most known Z-R equation, also known as the Marshal–Palmer equation, with (a, b) = (200, 1.6) is used. Although weather surveillance radars can provide an accurate estimation of precipitation at fine spatial resolutions ($1 \times 1\ km^2$) and temporal resolutions (10 minutes for clear-air mode, 6 minutes for precipitation mode), they are prone to several problems such as beam blockage at mountainous areas, three-body scatter spike and bright banding. Hence, downscaling methods are needed to enhance the resolution of outputs that are provided from satellites and numerical models when there is a shortage of acceptable images.

Data

The data-set (NEXRAD level III) used in this study was selected from 18,000 images provided by the National Climatic Data Center (NCDC) at www.ncdc.noaa.gov/cdo-web. The four events analyzed here were selected based on radar coverage and spatial structure of rainfall. The motivation behind the selected events was to examine the scaling behavior of rainfall fields in diverse forms of precipitating clouds. A brief explanation of these events and their reflectivity fields are given in Table 1 and Figure 1.

Table 1 | Description of study rainfall events

Event	Description	Time of occurrence
1) Hurricane Matthew (HM)	A category 4 tropical cyclone that impacted Haiti, Cuba and the states of Georgia, Florida and South Carolina from the US which caused more than 15 billion dollars of damage and 600 deaths	2016/10/07
2) Illinois flooding and severe weather (IF)	A slow-moving storm system that created rainfall totals of 12–24 cm across northern and central Illinois. It resulted in approximately 1 billion dollars of damage and four deaths	2013/04/18
3) Squall line (SL)	Over 1,600 km long across the Gulf of Mexico and Eastern US	2013/01/30
4) Scattered rainfall field (SF)	Some random precipitating clouds over Alabama state	2013/02/17

Wavelet decomposition

Wavelet transform is a mathematical tool that can be used for better understanding of scaling behaviors in stochastic processes. One dimensional discrete wavelet transform can decompose each signal into two components of scaling and wavelet coefficients while a two-dimensional discrete wavelet transform creates three wavelet coefficients in

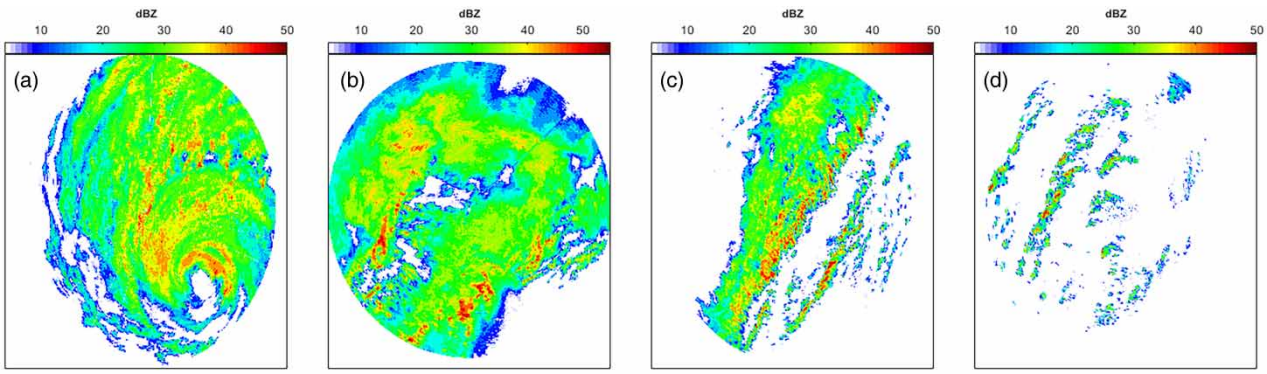

Figure 1 | Reflectivity field of (a) Hurricane Matthew (HM), (b) Illinois floods and severe weather (IF), (c) squall line (SL), (d) scattered rainfall field (SF).

each direction, i.e. horizontal, vertical and diagonal. In wavelet transform, various kernels can be used, but in this paper only the Haar kernel which serves as first-order difference discrete approximation was used due to its simple implementation, and the insensitivity of end results in the selected kernel (Perica & Foufoula-Georgiou 1996a).

Wavelet transform has another important property called dyadic sampling, meaning it reduces the resolution of a signal by two samples while doing the same for an image by 2×2 samples per each iteration. Because of this property, odd-sized images encounter size deformity in the process of upscaling and downscaling, so it is recommended to zero-pad the image until it can be dividable by 2^n, where n is defined as number of iterations to reach the required image resolution.

In this study, a two-dimensional wavelet transform was used to compute the scaling and wavelet coefficients of high-to-low resolution of the rainfall image which can be regarded as upscaling. By applying the high and low band-pass filters simultaneously to an image of size $2^{j+1} \times 2^{j+1}$ the directional wavelet coefficients and scaling coefficients are obtained as images in size of $2^j \times 2^j$. This process can be applied repeatedly in $j+1$ levels which finally results in an image of size 1×1.

Hence, by possessing all of the wavelet coefficients in all scales and scaling coefficients at the lowest resolution (highest scale), reconstruction of the image is achievable as (Ebtehaj & Foufoula-Georgiou 2010; Addison 2016):

$$S_{(j+1)}[2k, 2l] = \frac{S_j[k, l]}{2} + \frac{(T_{j,h}[k, l] + T_{j,v}[k, l] + T_{j,d}[k, l])}{2} \quad (1)$$

where S and T are approximation and wavelet coefficients, m is the resolution of the image, k and l stand for the pixel positions, h, v and, d, indicate the horizontal, vertical and diagonal wavelet coefficients, respectively. Here, $S_{(j+1)}[2k, 2l]$ implies that the size of higher resolution image is multiplied by a factor of two in each reconstruction step.

Standardized rainfall fluctuation

Investigations of directional wavelet coefficients of precipitation images revealed that a significant amount of them are very close to zero in the probability domain while having a thick tail probability distribution (Figure 2). Meaning, the probability distribution function is cusp shaped (see also, Ebtehaj & Foufoula-Georgiou 2011a, 2011b).

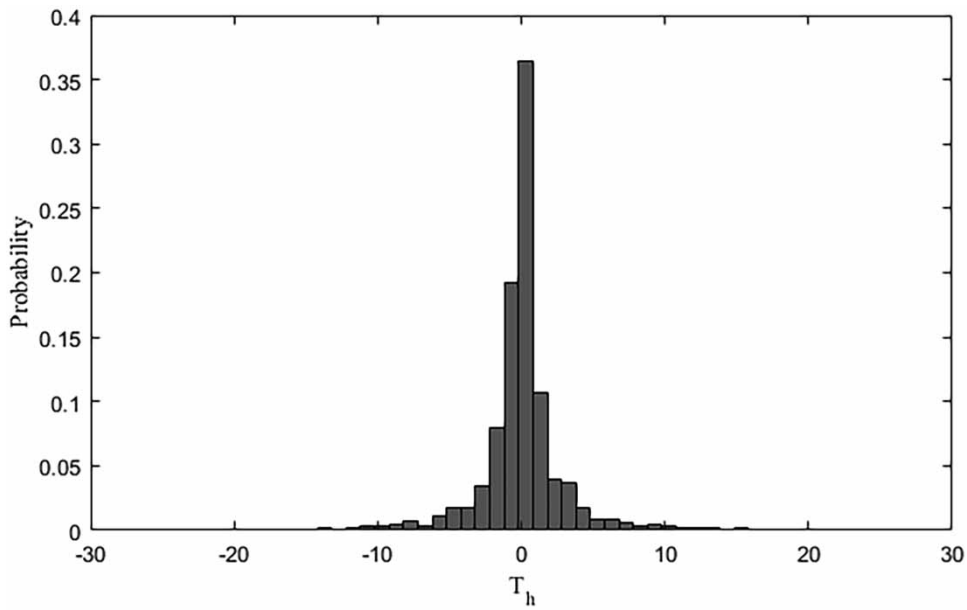

Figure 2 | Probability distribution of horizontal wavelet coefficient (T_h) of SL event for 2 km^2 resolution.

This specific behavior of rainfall in wavelet domain proves to be a troublesome problem. In order to overcome this issue, Perica & Foufoula-Georgiou (1996b) proposed a standardized rainfall fluctuation (SRF) concept meaning that wavelet coefficients are divided by their corresponding scaling coefficient which reduces the sparsity of wavelet coefficients, as:

$$\xi_{m+1(h,v,d)} = \frac{T_{m+1(h,v,d)}}{S_{m+1}} \tag{2}$$

where ξ is SRF, T and S are wavelet and approximation coefficients, m denotes the resolution and h, v, d are directions of wavelet coefficients. SRFs manifest themselves as a Gaussian distribution with zero mean. In other words, the standard deviations of these distributions are the only parameters worth exploring. Having only one parameter make SRFs a versatile tool that is simple to implement while providing attention to every aspect of the wavelet coefficients. Small values of standard deviation show that the field is not dispersed and the probability of higher intensity rainfall fields is lower, while larger values demonstrate the opposite concept.

Standard deviations of SRFs at various scales exhibit scaling behavior which can be expressed as:

$$\frac{\sigma_{\xi L_1}}{\sigma_{\xi L_2}} = \left(\frac{L_1}{L_2}\right)^H \tag{3}$$

where σ is standard deviation, H is the scale-independent variable, L_1 is the length (also width) of the pixel at lower resolution and L_2, is the length of the pixel at higher resolution. In this study, the length of each pixel is reduced by a factor of 2. Hence, Equation (3) can be written in the dyadic (base 2) form of:

$$\sigma_{\xi m+1,(h,v,d)} = \sigma_{\xi m_1,(h,v,d)}\, 2^{mH(h,v,d)} \tag{4}$$

It should be noted that higher values of H indicate a more significant degree of variability of the corresponding wavelet coefficient. Thus, they are more influential on extreme values of rainfall than others.

It is apparent that in radar imageries, a huge amount of non-rainfall values are background zeros that should be trimmed from the rest of the event for gaining a better comprehension. In the wavelet domain, background zeros in all wavelet and scaling coefficients remain zero whereas event-related zeros will turn into non-zero values in the upscaling procedure. In light of the above statement, the background zeros should be trimmed while trying to keep the event-related zeros.

Downscaling process

By acquiring the scale-independent parameter (H) and standard deviation of SRF ($\sigma_{\xi,(h,v,d)}$) at the lowest resolution, the downscaling process from low-resolution to high-resolution fields can be implemented.

The schematic process of the downscaling process is illustrated in Figure 3.

Downscaling process can be summarized in four steps as:

- For the image at lowest resolution, three Gaussian derived fields with the corresponding size to the lowest resolution image with zero mean and standard deviation of ($\sigma_{\xi_m,(h,v,d)}$) are generated. These fields are called generated SRFs.

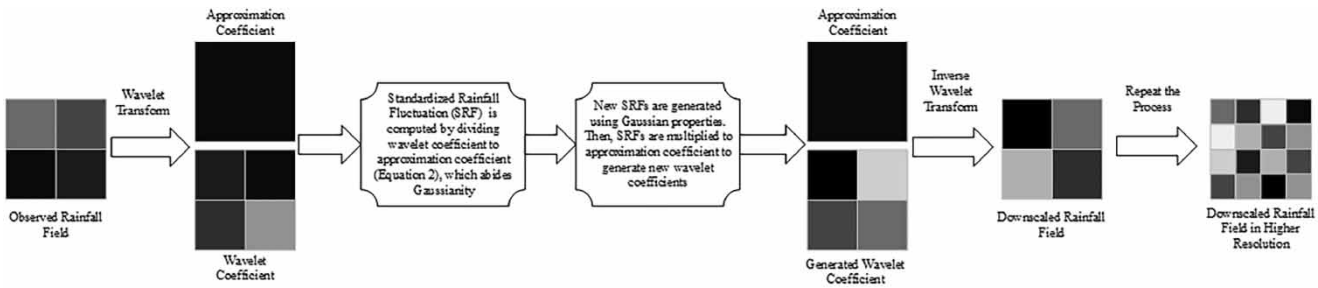

Figure 3 | Schematic implementation of downscaling process.

- By multiplying the three generated SRFs with the corresponding low-resolution image, three directional wavelet coefficients ($T_{m,(h,v,d)}$) are obtained (Equation (2)).
- Three directional wavelet coefficients and the low-resolution image are transformed into a higher resolution image via a two-dimensional inverse wavelet transform. In other words, for each pixel at a lower resolution, four other pixels are generated which increases the image size by a factor of 2×2 and enhances its resolution.
- The same procedure is repeated for the higher resolution image via $\sigma_{\xi m-1,(h,v,d)} = \sigma_{\xi m,(h,v,d)} 2^{-H(h,v,d)}$. So, in each repetition, the power of two will increase by the amount of one.

RESULTS AND DISCUSSION

The proposed downscaling method was applied to the mentioned rainfall events (Table 1) to analyze the discrepancies between model output and observed rainfall data. As mentioned before, the downscaling process is not applicable unless the SRFs, which result from dividing a directional wavelet coefficient to its corresponding scaling coefficients, have Gaussian distribution with zero mean where their standard deviations show scaling behavior. As illustrated in Figure 4, there are some variations between Gaussian and SRFs distributions for an SL event, which are mostly placed adjacent to the center of the probability distribution function. These variations may cause inconsistency in modeling since they are close to zero which fails to have a significant impact on the downscaled rainfall field. In view of the above statement and the fact that tails of distribution which correspond to extreme values of rainfall is recognized in SRFs, it is obvious that Gaussian distribution is an appropriate fit for SRFs.

In order to examine the scaling behavior of SRFs, their standard deviations are plotted over a wide range of scales. It must be emphasized that scaling characteristics of SRFs exhibit a linear relationship between a scale-independent variable versus scale in a semi-log plot which is illustrated for an SL event (as an example) in Figure 5.

It must be noted that the scaling behavior of SRFs in some of the events, specifically the SF event, at scales larger than $16 \times 16\ \text{km}^2$ ($m = 4$) started to show deviations from linearity which in order to have a uniform set of

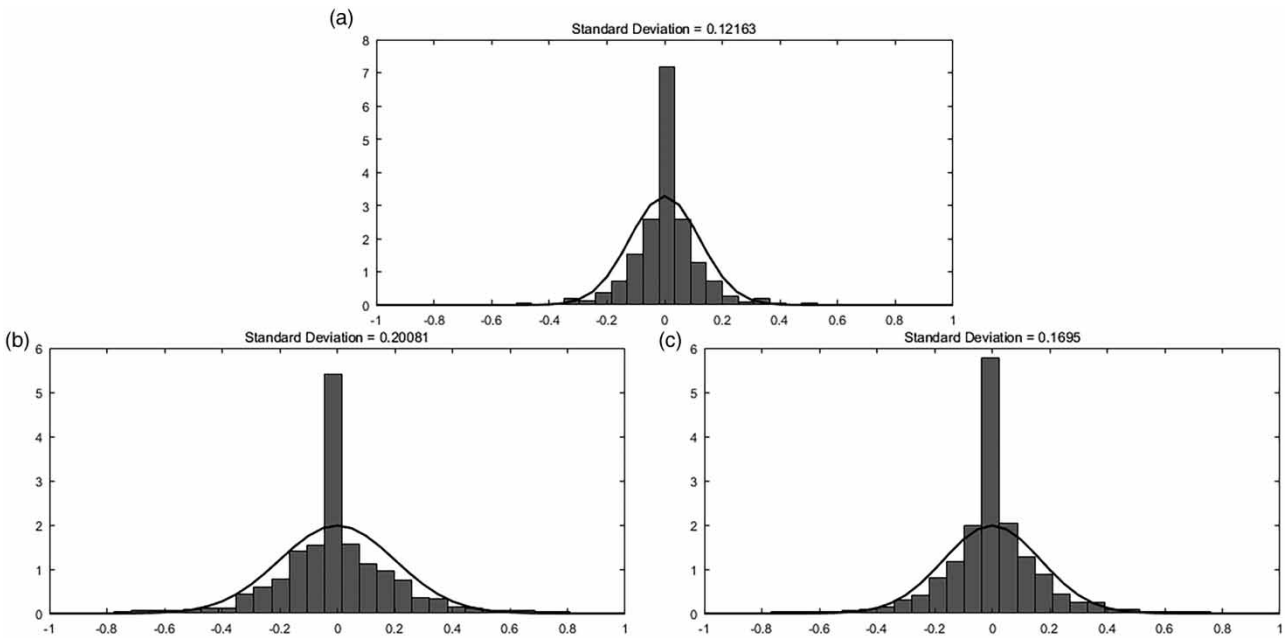

Figure 4 | Probability distribution of SRF of SL event for 2 km^2 resolution for each direction: (a) diagonal, (b) vertical, (c) horizontal.

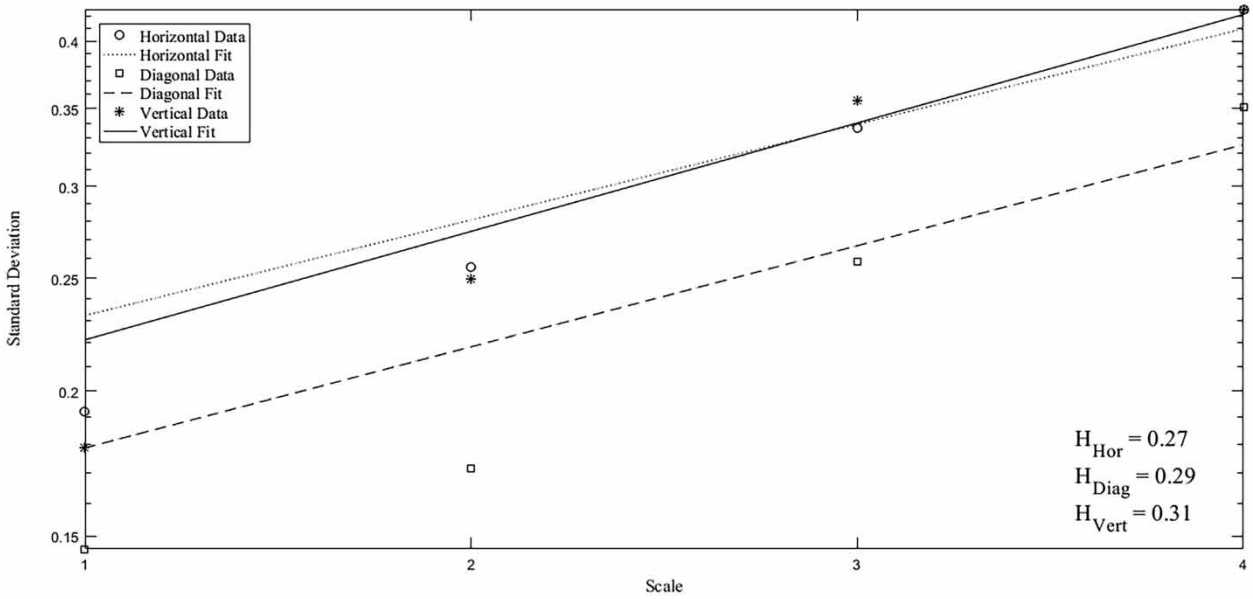

Figure 5 | Semi-log plot of standard deviation of SRF for SL event.

resolutions for all events, the aggregation procedure should be finished at this resolution. The reason for deviation of the SF event sooner than other events originates from its core properties, which only have a few maximum values.

After acquiring the scale-independent parameter (H) and standard deviation of SRF (σ_ξ) at the lowest resolution, the downscaling scheme from low-resolution to high-resolution field could be implemented (Table 2).

After careful consideration it was seen that generated rainfall fields have the potential to improve which is addressed in succeeding paragraphs. In the downscaling procedure there is a considerable chance of generating negative rainfall fields. After careful observation of negative values, it was seen that negative fields with a higher gradient tend to be adjacent to high gradient positive fields which caused considerable noise in the downscaled rainfall field. In order to overcome this problem, negative values were given a random value between zero and the lowest value of four generated pixels (lowest values were chosen to ensure rainfall extremes stay intact). Afterward, the three adjacent pixels that were generated in the downscaling process were evenly reduced in a manner to conserve the mean (after subtracting this value from adjacent pixels there is still a slight chance of creating negative values which was solved by reducing the random value by the amount of a unit). This procedure was carried out in parallel with the work of Harris & Foufoula-Georgiou (2001), with one exception that they changed the negative values to zero instead of substituting them with a positive value where this modification could lead to gaps in the rainfall field in which these gaps may be enlarged through the following computation iterations and introduce voids in the spatial structure of the rainfall field. Applying this specific modification managed to increase the visual resemblance of observed rainfall to generated rainfall fields while maintaining statistical coefficient values.

Spatial rainfall observations show that rainfall exhibits cluster-like behavior (e.g. LeCam 1961; Gupta & Waymire 1990). In other words, high-intensity rainfall fields (high gradient cells) are within other regions of low-intensity rainfall fields (low gradient cells). Furthermore, the downscaling process is unable to save pixel location which results in

Table 2 | Estimated parameters in the downscaling process for the events

Rainfall event	$H_{Diagonal}$	$H_{Vertical}$	$H_{Horizontal}$	$\sigma_{4,\ Diagonal}$	$\sigma_{4,\ Vertical}$	$\sigma_{4,\ Horizontal}$
HM	0.19	0.28	0.21	0.19	0.29	0.26
IF	0.24	0.27	0.26	0.21	0.28	0.32
SF	0.31	0.3	0.29	0.49	0.62	0.57
SL	0.29	0.31	0.27	0.33	0.42	0.40

the relocation of rainfall pixels to adjacent cells. These facts motivated us to create a kernel that finds and sorts the maximum values of non-overlapped 5×5 samples and randomly places the second-highest value next to the maximum value, and so on. The reason for not choosing an overlapping kernel is directly caused by continuous displacement of rainfall maxima which altered the generated rainfall fields inconsistent with observed rainfall fields.

By applying this non-overlapping kernel, high-gradient pixels were placed next to each other to create rainfall clusters. Moreover, this kernel managed to reduce the blockiness of the image to some extent, particularly at rainfall field boundaries which have lower variability compared to the other zones of the rainfall field. Employing this modification produced clusters of rainfall which is one of the most important features of high-resolution rainfall fields.

The downscaling process was applied to four upscaled events at 16×16 km^2 until reaching the original resolution of 1×1 km^2. The model output (simulated) has some variations in each run of the downscaling process whereby in order to minimize such variations, the average of ten independent simulations (S_{10}) was taken into consideration for computing the performance criteria.

One of the main tools for examining the scaling behavior of rainfall fields in a wide range of scales is Power Spectrum. Two-dimensional power spectrum employs Fourier transform which grants it the ability to examine the rainfall field in the frequency domain. In order to obtain a better understanding of the rainfall field in the Fourier domain, the field was logarithmically transformed. Afterward, the power spectra of these log-transformed rainfall fields were computed which exhibit the energy division between low and high-frequency intensities.

The two-dimensional power spectrum can be reduced into a one-dimensional spectrum by performing a rotational average within the two-dimensional domain which presents itself as linearity in log-log scales. Empirically, some researchers confirmed that the spectral power of rainfall fields falls with the frequency which abides the power-law scaling relationship in the form of (Tolhurst *et al.* 2007):

$$P(f_r) \propto \frac{1}{f_r^{\beta}} \tag{5}$$

where f_r and β are radial frequency and drop-off rate, respectively.

The logic behind this behavior has been the subject of few debates. Some of the works carried out in this area connected this behavior to the turbulence properties of the rainfall (Schertzer & Lovejoy 1991).

The variability of a rainfall field is linked to the drop-off rate of its power spectrum in which the smoother field demonstrates larger values of drop-off rate and vice versa. The importance of this property is emphasized in the downscaling process which is usually varied with the resolution enhancement.

The drop-off rate of the events for one simulation (S_1) and the average of ten simulations (S_{10}) for 1×1 km^2 are reported in Table 3 for all events.

According to Table 3, the drop-off rate of one simulation for all events, with the exception of the SF event, is smaller than the observed field which implies that the observed field is smoother than the simulated field. Moreover, the drop-off rate of S_{10} is much larger than the corresponding values which is caused by averaging ten different simulations. Figure 6 illustrates a one-dimensional power spectrum for the SL event for the log-transformed average of S_{10}, S_1 and observed fields at 1 km^2 resolution.

Further evaluation of the downscaling process was carried out using correlation coefficient (CC) between simulated fields at each scale with their corresponding observations, as:

$$CC = \frac{\sum_i \sum_j (A_{ij} - \overline{A})(B_{ij} - \overline{B})}{\sqrt{\left(\sum_i \sum_j (A_{ij} - \overline{A})^2\right)\left(\sum_i \sum_j (B_{ij} - \overline{B})^2\right)}} \tag{6}$$

Table 3 | Drop-off rates of power spectrums for highest resolution

Event	O	S_1	S_{10}
HM	2.43	1.99	3.13
IF	2.55	2.05	2.85
SL	2.11	2.03	3.07
SF	1.01	1.25	1.38

O, Observed; S_1, One simulation; S_{10}, Average of ten simulations.

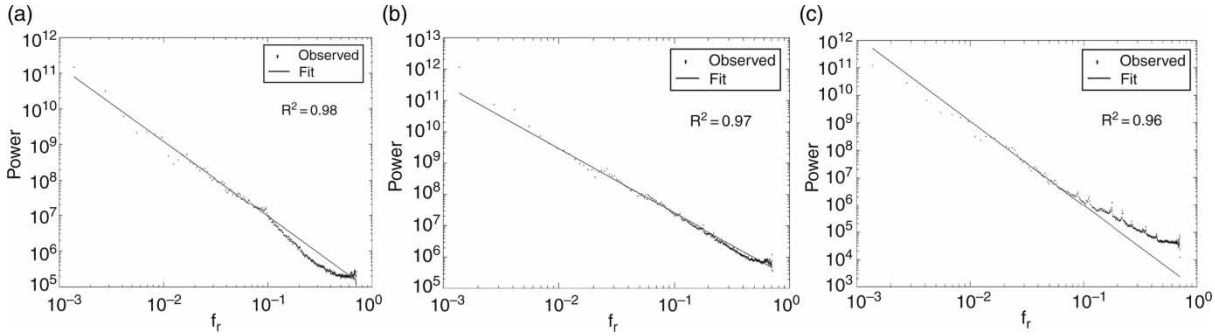

Figure 6 | One dimensional power spectrum of SL event for: (a) observed, (b) S_1, (c) S_{10}.

where A, B, $\bar{A}$, $\bar{B}$, i, j and CC are observed field, simulated field, mean of the observed field, mean of the simulated field, location of the pixel and correlation coefficient, respectively.

By plotting the resulted CC values versus scales, the variation trend in all scales for the four events can be seen. By examining Figure 7, it is evident that higher resolution images tend to get smaller values of CC which results from introducing deviation to the downscaled field in each iteration.

For analyzing the accuracy of the downscaling process, mean and standard deviation values of simulated fields were compared with those of observation fields. As can be seen from Table 4, simulations of the rainfall field estimate the mean and standard deviation relatively close to the observed values with the exception of the SF event. Evidently, S_{10} shows smaller values of mean and standard deviation compared to S_1 which is caused by smoothing the rainfall field via averaging. This property is also seen in the drop-off rate of power spectra which showed that S_1 has a higher degree of variability in contrast to S_{10}. Another important point is that even though the averages of obtained results are close to the observational averages they are underestimated, while standard deviations for most of the cases are overestimated. This evidence is a direct consequence of SRFs inadequacies. Even though SRFs manage to encompass a large portion of sparsity and thick-tails of wavelet coefficients distribution within themselves, there is still a minor part that is of sparsity in the distribution.

In order to further analyze the reliability of the downscaling process, intensities of rainfall fields were sorted in ascending order, afterward the determination coefficient (DC) of S_1 versus observed rainfall field for the events at all scales were computed via Equation (7) which is reported in Table 5:

$$DC = 1 - \frac{\sum (A_i - B_i)^2}{\sum (A_i - \overline{B}_i)^2} \tag{7}$$

Determination coefficient varies from $-\infty$ to 1, where 1 implies the exact resemblance between the observed and simulated field, while correlation coefficient values vary in the range of -1 to 1, where 1 indicates that the dispersion of the simulated field is equal to the observed field. Furthermore, CC tends to adjust itself around extreme outliers which may apply bias along high values, which is also true for DC since squared differences are more pronounced in extreme values while neglecting low values (Legates & McCabe 1999). In addition, scatterplots of all events at the 2×2 km^2 scale are illustrated in Figure 8.

As can be seen in Figure 8, different rainfall values have been generated for a unique observed rainfall value which is rooted in rounding reflectivity fields (NEXRAD level III) in 5 dBZ increments which results in discrete observation values even after transforming reflectivity rainfall fields to rainfall rates. Another important feature of Figure 8 is the discrepancy between high-intensity rainfall values due to the overestimation of standard deviation in the downscaling process (Table 4). Since SRFs are unable to completely absorb all of the properties of wavelet coefficients, especially thick-tails of distribution, standard deviations of the simulated values are higher than those of the observed values. Moreover, these standard deviations are iterated for each resolution which converts extreme values to even higher

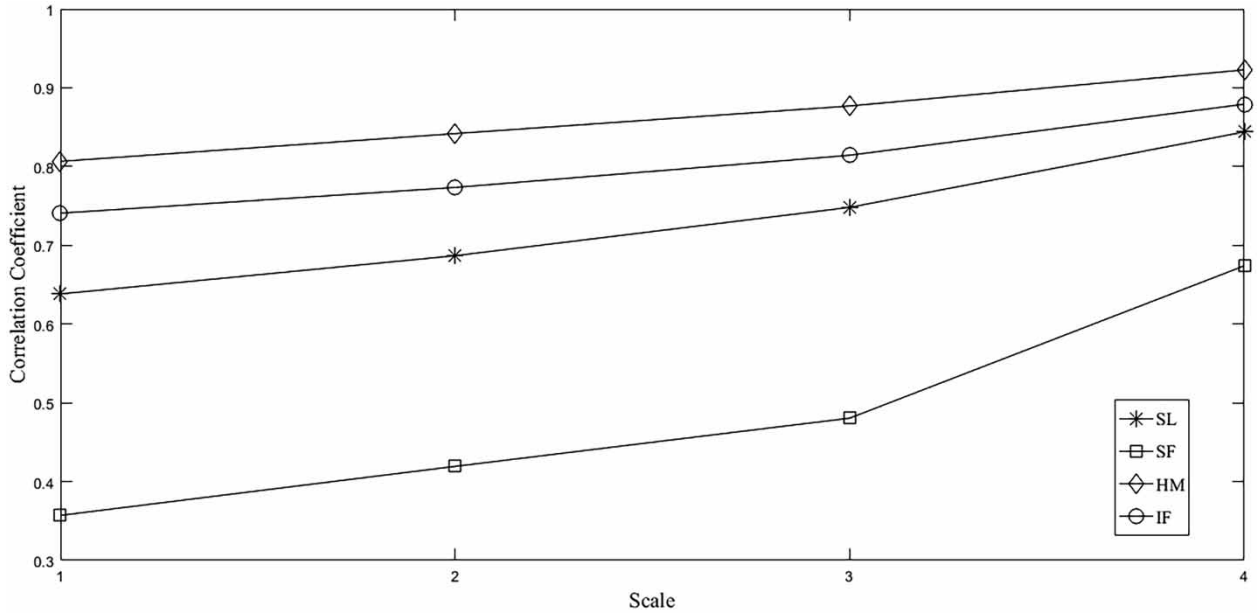

Figure 7 | Correlation coefficient of observational and simulated fields at different scales for all four events.

Table 4 | Statistical moments for the four events at all scales

Statistical moments		Scale (pixel size in km²)				
		1×1	2×2	4×4	8×8	16×16
μ_{HM}	O	3.13	6.02	11.47	21.54	39.65
	S_1	2.74	5.43	10.65	20.69	
	S_{10}	2.49	4.93	9.8	19.66	
σ_{HM}	O	2.8	5.33	10.19	19.31	35.9
	S_1	3.29	6.24	11.76	21.57	
	S_{10}	2.35	4.64	9.15	18.1	
μ_{IF}	O	4.01	7.75	14.76	27.78	51.67
	S_1	3.46	6.87	13.55	26.59	
	S_{10}	3.22	6.41	12.8	25.67	
σ_{IF}	O	5.01	9.53	17.96	32.77	57.67
	S_1	5.23	9.95	18.81	34.29	
	S_{10}	3.66	7.23	14.29	28.41	
μ_{SF}	O	2.98	4.56	6.26	7.89	9.54
	S_1	0.73	1.44	2.82	5.44	
	S_{10}	0.4	0.82	1.75	4.04	
σ_{SF}	O	4.56	7.64	11.82	15.92	19.39
	S_1	2.46	4.45	7.81	13.11	
	S_{10}	1.02	1.93	3.91	8.32	
μ_{SL}	O	3.35	6.23	11.23	19.59	32.23
	S_1	2.34	4.59	8.92	17.23	
	S_{10}	1.96	3.87	7.71	15.68	
σ_{SL}	O	4.23	7.56	13.92	23.66	38.36
	S_1	4.35	7.94	14.3	24.7	
	S_{10}	2.55	4.94	9.6	18.92	

O, Observed; S_1, One simulation; S_{10}, Average of ten simulations.

Table 5 | Determination coefficients of events at all scales

Scale (km)	HM	IF	SF	SL
1×1	0.9	0.93	0.84	0.92
2×2	0.95	0.97	0.9	0.98
4×4	0.97	0.98	0.93	0.99
8×8	0.98	0.99	0.97	0.99

values which shifts the points to the positive direction of the y-axis in the scatterplot. It is evident from Table 5 that determination coefficients are in the vicinity of one which implies that rainfall intensities are well captured in simulation. Despite the previous remark, rainfall intensities can shift to the neighboring pixels. Moreover, it can be seen that high-resolution rainfall fields have lower determination coefficients which can be explained by repeated iteration of the downscaling process which subjected the field to deviations. In other words, even small deviations at lower resolutions can transfer to higher resolutions while having their own deviations. Sources of these deviations can be traced back to inconsistencies of assumption of the Gaussian distribution for SRFs (Figure 4) as well as discrepancies of data and its corresponding linearity in scaling behavior (Figure 5). By considering the evaluation criteria and their union in showing the SF event to be poorly simulated, it is

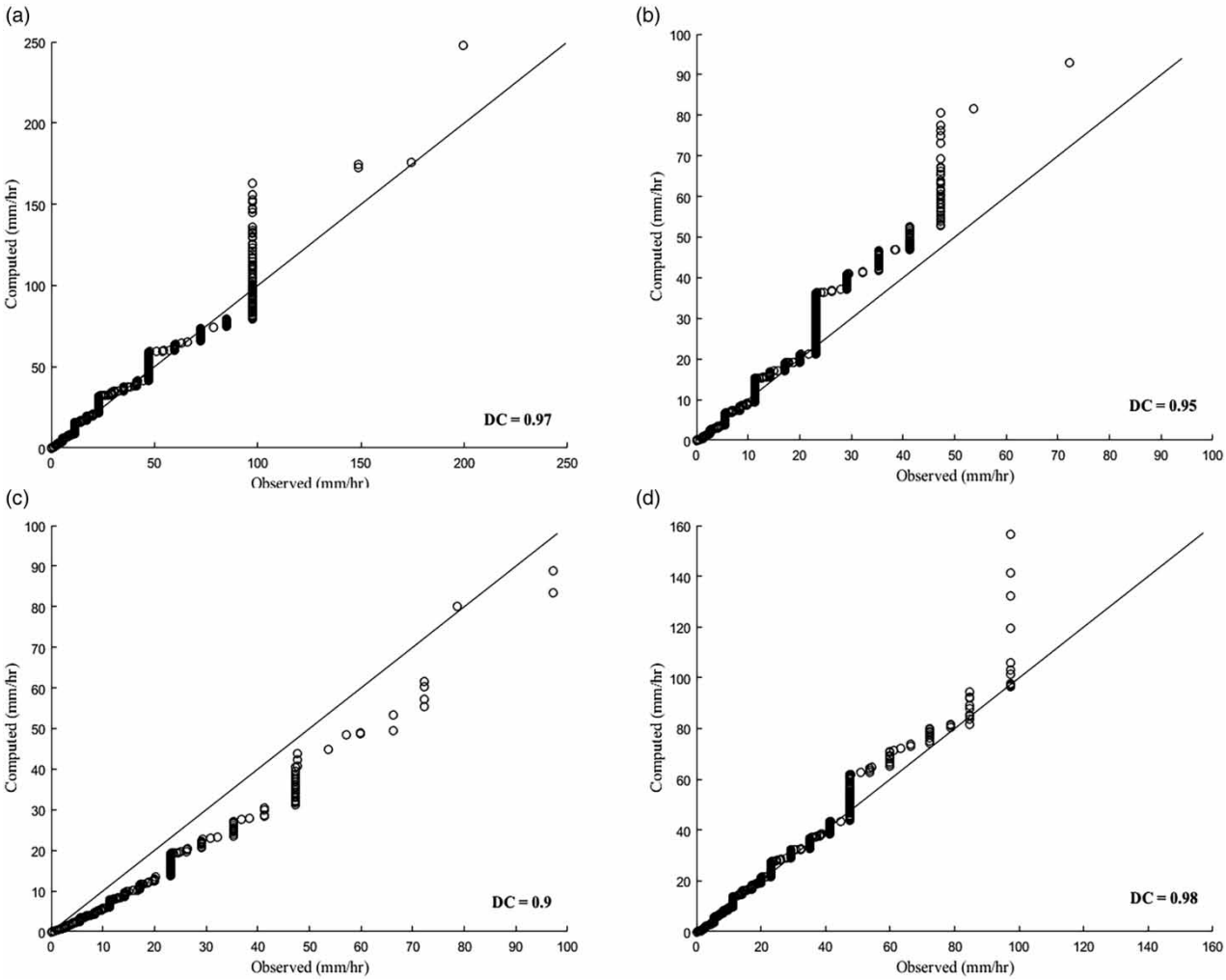

Figure 8 | Scatter plots of events: (a) IF, (b) HM, (c) SF and (d) SL at 2 km^2 resolution.

understood that the downscaling method is unable to recreate such events and the reason behind this matter is related to its spatial structure and sparsity of rainfall event in radar range. Moreover, the SF event faces a shortage of high-intensity rainfall cells compared to the other events which translates into thinner tails and sharper cusps for approximation coefficients and directional wavelet coefficients. This indicates that standardizing directional wavelet coefficients for an SF event is unable to reduce the sparsity and also it is incapable of handling thick-tailed properties of directional wavelet coefficients to the same extent as other events (Perica & Foufoula-Georgiou 1996a).

The spatial structure of the SL event for S_{10} and observed fields in all resolutions is illustrated in Figure 9. It is apparent from Figure 9 that the proposed model can create almost similar spatial patterns that have the ability to reproduce clusters of rainfall while keeping the rainy fraction intact. It is worth noting that this similarity is much better at low resolutions compared to higher resolutions, which is also implied in the aforementioned evaluation criteria.

CONCLUDING REMARKS

The study of rainfall downscaling is rooted in the necessity to gain knowledge about precipitation in finer resolutions to improve long-term water management on local scales (Cheng *et al.* 2005; Fotovatikhah *et al.* 2018). Four radar-

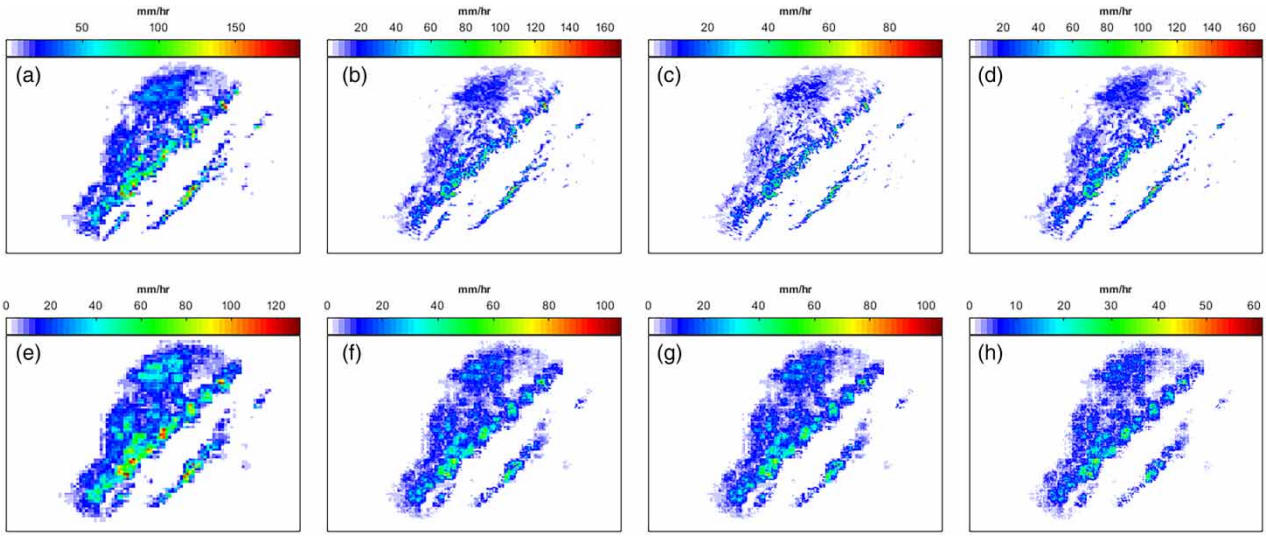

Figure 9 | Spatial structure of observed SL event at: (a) 8×8 km^2, (b) 4×4 km^2, (c) 2×2 km^2, (d) 1×1 km^2 and S_{10} at (e) 8×8 km^2, (f) 4×4 km^2, (g) 2×2 km^2, (h) 1×1 km^2.

derived events (NEXRAD level III) with different structures were chosen in this study to be examined for investigation of scaling behavior in the wavelet domain. Wavelet coefficients mostly consist of values close to zero while a few extreme values contain a large bulk of the rainfall energy. In order to deal with this, standardized rainfall fluctuation (SRF) was presented which resembled Gaussian distribution with zero mean. Standard deviations of the distributions showed scaling behavior at scales varying between $m = 1$ until $m = 4$ (1–16 km^2). After estimating the scale-independent variable (H) and the standard deviation of SRF at lowest resolutions, the process of downscaling rainfall was performed via inverse wavelet transform. Generated fields were modified by removing negative values and recreating the cluster behavior of rainfall to further enhance the ability of the model for the reproduction of the simulated rainfall fields.

The energy distributions of the simulated fields were compared with the observation fields using a power spectrum which is evident from the drop-off rate of these spectrums. For all of the events, with the exception of the SF event, the drop-off rate of observation is higher than simulated which implies that the simulated field has a higher degree of variability. The simulated fields were also evaluated by comparing first and second-order moments that were preserved at all scales for the three events of SL, HM, and IF. In addition, values of the determination coefficient clearly suggest the fact that all of the rainfall fields have almost the same intensities, even if these values are transferred to adjacent pixels. It must be noted that spatial properties of rainfall, such as high-gradient clusters and fraction of the wetted area, are similar to those of the observation fields. The inability of the model to correctly simulate the SF event is deeply rooted in the intensity of rainfall cells, as well as the inadequacy of SRFs to modulate sparsity of directional wavelet coefficients.

The results of the proposed downscaling process in most of the aspects show similarity with the observed rainfall fields. However, in order to remove the drawbacks of this process and offer new grounds for investigation, it is recommended to investigate scaling behavior in high-order statistical moments such as skewness and kurtosis as well as fitting other density functions to the directional wavelet functions to see if they can reproduce its features or not.

REFERENCES

Addison, P. S. 2016 *The Illustrated Wavelet Transform Handbook: Introductory Theory and Applications in Science, Engineering, Medicine and Finance*. CRC Press, Boca Raton, USA.

Aghakouchak, A., Bárdossy, A. & Habib, E. 2010 Conditional simulation of remotely sensed rainfall data using a non-Gaussian v-transformed copula. *Adv. Water Resour.* **33** (6), 624–634.

Baghanam, A. H., Nourani, V., Keynejad, M. A., Taghipour, H. & Alami, M. T. 2019 Conjunction of wavelet-entropy and SOM clustering for multi-GCM statistical downscaling. *Hydrol. Res.* **50** (1), 1–23.

Berne, A. & Krajewski, W. F. 2013 Radar for hydrology: unfulfilled promise or unrecognized potential? *Adv. Water Resour.* **51**, 357–366.

Cammalleri, C., Anderson, M. C., Gao, F., Hain, C. R. & Kustas, W. P. 2013 A data fusion approach for mapping daily evapotranspiration at field scale. *Water Resour. Res.* **49** (8), 4672–4686.

Cheng, C. T., Lin, J. Y., Sun, Y. G. & Chau, K. 2005 Long-term prediction of discharges in Manwan Hydropower using adaptive-network-based fuzzy inference systems models. In: *International Conference on Natural Computation*. Advances in Natural Computation, Springer, Germany, pp. 1152–1161.

Chow, V. T., Maidment, D. R. & Mays, L. W. 1988 *Applied Hydrology. Water Resources and Environmental Engineering*. McGraw-Hill, New York.

Cowpertwait, P. S. P., Oconnell, P. E., Metcalfe, A. V. & Mawdsley, J. A. 1996 Stochastic point process modeling of rainfall. 2. Regionalization and disaggregation. *J. Hydrol.* **175** (1–4), 47–65.

Ebtehaj, M. & Foufoula-Georgiou, E. 2010 Orographic signature on multiscale statistics of extreme rainfall: a storm-scale study. *J. Geophys. Res.* **115** (D23), D23112.

Ebtehaj, M. & Foufoula-Georgiou, E. 2011a Adaptive fusion of multisensor precipitation using Gaussian-scale mixtures in the wavelet domain. *J. Geophys. Res. Atmos.* **116** (D22), D22110.

Ebtehaj, M. & Foufoula-Georgiou, E. 2011b Statistics of precipitation reflectivity images and cascade of Gaussian-scale mixtures in the wavelet domain: a formalism for reproducing extremes and coherent multiscale structures. *J. Geophys. Res. Atmos.* **116** (14), D14110.

Farboudfam, N. & Nourani, V. 2018 Wavelet-based multi station disaggregation of rainfall time series in mountainous regions. *Hydrol. Res.* **50** (2), 545–561.

Fotovatikhah, F., Herrera, M., Shamshirband, S., Chau, K. W., Faizollahzadeh Ardabili, S. & Piran, M. J. 2018 Survey of computational intelligence as basis to big flood management: challenges, research directions and future work. *Eng. Appl. Comput. Fluid Mech.* **12** (1), 411–437.

Gupta, V. K. & Waymire, E. 1990 Multiscaling properties of spatial rainfall and river flow distributions. *J. Geophys. Res.* **95** (D3), 1999–2009.

Harris, D. & Foufoula-Georgiou, E. 2001 Subgrid variability and stochastic downscaling of modeled clouds: effects on radiative transfer computations for rainfall retrieval. *J. Geophys. Res. Atmos.* **106** (D10), 10349–10362.

Joss, J. & Waldvogel, A. 1990 Precipitation measurement and hydrology. In: *Radar in Meteorology* (J. Joss, A. Waldvogel & C. G. Collier, eds). American Meteorological Society, Boston, MA, pp. 577–606.

Kang, B. & Ramrez, J. A. 2010 A coupled stochastic space-time intermittent random cascade model for rainfall downscaling. *Water Resour. Res.* **46** (10), W10534.

Koutsoyiannis, D. & Onof, C. 2001 Rainfall disaggregation using adjusting procedures on a Poisson cluster model. *J. Hydrol.* **246** (1–4), 109–122.

Kumar, P. & Foufoula-Georgiou, E. 1993a A multicomponent decomposition of spatial rainfall fields: 1. Segregation of large- and small-scale features using wavelet transforms. *Water Resour. Res.* **29** (8), 2515–2532.

Kumar, P. & Foufoula-Georgiou, E. 1993b A multicomponent decomposition of spatial rainfall fields: 2. Self-similarity in fluctuations. *Water Resour. Res.* **29** (8), 2533–2544.

LeCam, L. 1961 A stochastic description of precipitation. In: *Proceedings of the Fourth Berkeley Symposium on Mathematical Statistics and Probability*, Vol. 3. University of California Press, USA, pp. 165–186.

Legates, D. R. & McCabe, G. J. 1999 Evaluating the use of 'goodness-of-fit' measures in hydrologic and hydroclimatic model validation. *Water Resour. Res.* **35** (1), 233–241.

López López, P., Immerzeel, W., Rodríguez Sandoval, E., Sterk, G. & Schellekens, J. 2018 Spatial downscaling of satellite-based precipitation and its impact on discharge simulations in the Magdalena River Basin in Colombia. *Front. Earth Sci.* **6** (68), 1–23.

Lovejoy, S. & Schertzer, D. 1990 Multifractals, universality classes and satellite and radar measurements of cloud and rain fields. *J. Geophys. Res.* **95** (D3), 2021–2034.

Nourani, V. & Farboudfam, N. 2019 Rainfall time series disaggregation in mountainous regions using hybrid wavelet-artificial intelligence methods. *Environ. Res.* **168**, 306–318.

Olsson, J. 1995 Limits and characteristics of the multifractal behavior of a high-resolution rainfall time series. *Nonlinear Process. Geophys.* **2** (1), 23–29.

Ormsbee, L. E. 1989 Rainfall disaggregation model for continuous hydrologic modeling. *J. Hydraul. Eng.* **115** (4), 507–525.

Perica, S. & Foufoula-Georgiou, E. 1996a Linkage of scaling and thermodynamic parameters of rainfall: results from midlatitude mesoscale convective systems. *J. Geophys. Res. Atmos.* **101** (D3), 7431–7448.

Perica, S. & Foufoula-Georgiou, E. 1996b Model for multiscale disaggregation of spatial rainfall based on coupling meteorological and scaling descriptions. *J. Geophys. Res.* **101** (D21), 26347–26361.

Rebora, N., Ferraris, L., Von Hardenberg, J. & Provenzale, A. 2006 Rainfall downscaling and flood forecasting: a case study in the Mediterranean area. *Nat. Hazards Earth Syst. Sci.* **6** (4), 611–619.

Rodriguez-Iturbe, I., Cox, D. R. & Isham, V. 1987 Some models for rainfall based on stochastic point processes. *Proc. R. Soc. A Math. Phys. Eng. Sci.* **410** (1839), 269–288.

Rodriguez-Iturbe, I., Cox, D. R. & Isham, V. 1988 A point process model for rainfall: further developments. *Proc. R. Soc. A Math. Phys. Eng. Sci.* **417** (1853), 283–298.

Schertzer, D. & Lovejoy, S. 1991 Nonlinear geodynamical variability: multiple singularities, universality and observables. In: *Non-Linear Variability in Geophysics*

(D. Schertzer & S. Lovejoy, eds.). Springer Netherlands, Dordrecht, pp. 41–82.

Singh, V. P. 1997 Effect of spatial and temporal variability in rainfall and watershed characteristics on stream flow hydrograph. *Hydrol. Process.* **11** (12), 1649–1669.

Singh, V. P. & Chowdhury, P. K. 1986 Comparing some methods of estimating mean areal rainfall. *J. Am. Water Resour. Assoc.* **22** (2), 275–282.

Tolhurst, D. J., Tadmor, Y. & Chao, T. 2007 Amplitude spectra of natural images. *Ophthal. Physiol. Optics* **12** (2), 229–232.

Venugopal, V., Roux, S. G., Foufoula-Georgiou, E. & Arneodo, A. 2006 Revisiting multifractality of high-resolution temporal rainfall using a wavelet-based formalism. *Water Resour. Res.* **42** (6), W06D14.

World Meteorological Organization (WMO) 2008 *Guide to Meteorological Instruments and Methods of Observation*, 7th edn. WMO-No 9. WMO, Geneva.

First received 23 October 2019; accepted in revised form 26 January 2020. Available online 27 March 2020